6.5 Proton Ring Optics

6.5.1 Introduction

The concept for a new HERA interaction region as presented in section **??** is to provide an early separation of the colliding proton- and electron beam. For this purpose space is needed close to the interaction points to install magnets as close as possible to the interaction point. In this section the optimization of the beam optics for the HERA proton ring will be described. For the considered geometry of the interaction regions in the HERA straight sections NORTH and SOUTH and with the foreseen parameters of the new designed magnets an optical solution has to be found which matches the conditions of the beam collision points to the parameters in the arcs.

In the case of the optics for luminosity operation the main goal is to achieve the smallest possible beam dimensions at the interaction point. The main boundary conditions are the free aperture in the low beta quadrupoles that has to be guaranteed for high beam lifetime and small backgrounds close to the IP's and the contribution of chromatic effects rising from the mini-beta insertion sections.

For small beam energies close to the flat bottom energy of $E_{inj} = 40\,GeV$, the emittance of the proton beam is large. Therefore the betafunctions must be kept small inside the interaction region and the beam optics has to be optimised for the purpose of aperture limitations and lifetime considerations.

Thus it turns out that more or less in the same manner as the HERA-proton ring is running at present a variety of optical solutions have to be found that cover the whole energy range of the accelerator and that fulfill the required conditions in each part.

6.5.2 Luminosity Optics

For the desired luminosity enhancement the considered beta function at the interaction point β^* is ${\beta^*}_x = 2.45$m in the horizontal plane and ${\beta^*}_y = 0.18$m in the vertical plane. As the collision points of the machine represent the optical symmetry points, the derivative of the beta function has to vanish and we have to deal with optical parameters at the IP's as presented in table 16.

	beta function	alfa function	dispersion	derivative of dispersion
horizontal	2.45 m	0.0	0.0 m	0.0
vertical	0.18 m	0.0	0.0 m	0.0

Table 16: *Optical parameters at the interaction points NORTH and SOUTH used in the luminosity upgrade study*

In Fig. 35 the lattice of the proton magnet structure in the new designed interaction region is shown (top view). It includes the quadrupole magnets that are designed for the focusing of the electron beam but they act on the protons as well. The transverse dimensions of the magnets have been properly scaled to the extend they are defined at the present state of the design. For clarity only the proton beam line is shown. The lattice changes are restricted to a region of $\pm 55\,m$ distance from the interaction point. The vertical bend of the proton ring and the insertion had to be matched geometrically to the existing HERA machine.

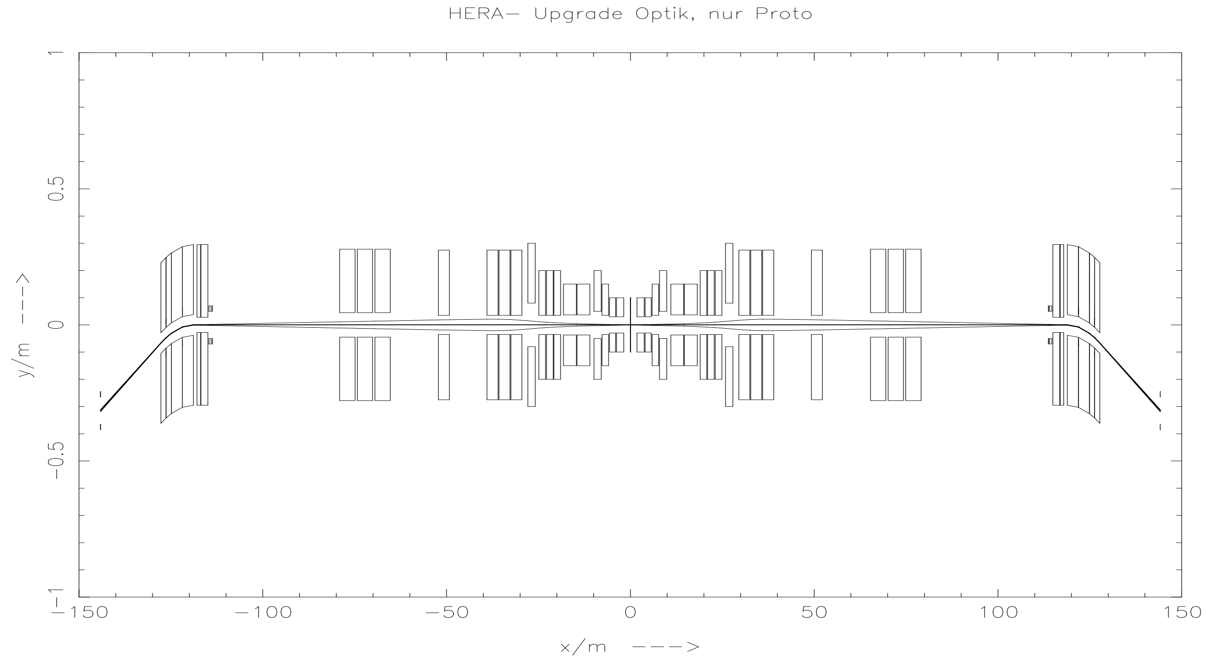

Figure 35: *Magnet lattice of the new designed interaction region. The magnets are shown for the luminosity case with the above mentioned optical parameters at the interaction point and for clarity only the proton beam is shown.*

From the optics point of view the first magnets named 'QG/QH, QI, QJ' are acting as triplet focusing magnets on the electron beam. But since the beams are not separated inside these segments they have to be taken into account for the proton luminosity optics and their influence is included —scaled with the ratio of the beam energies $30\,GeV/820\,GeV$ as boundary condition in the optical calculations mentioned below.

Except for this weak early focusing of the electron triplet, the proton beam is focused with the help of the magnets 'QM1 and QM2', 'QN' and the 'QR'–type magnets which are forming a doublet structure. The first magnets 'QM' and 'QN' provide vertical focusing. They limit the increase of the vertical beta function to a level of 1600 m. After the vertical focusing elements the horizontal beta function is controlled by the 'QR'–type quadrupoles QR1 ... QR3. The maximum value achieved there is about $\beta_x \approx 1900\,\mathrm{m}$.

The horizontally focusing magnets are spread over a distance of about 20 m in order to provide the flexibility needed for the low energy optics that will be discussed below. Nevertheless, the focusing center of the four horizontally focussing quadrupoles is kept as close as possible to the IP, namely in a distance of 40 m where the horizontal beta function reaches its maximum and starts to decrease again.

In Fig. 36 these main features of the new lattice embedded inside the existing HERA-proton ring is visualized. In the upper part of the plot the horizontal and vertical beta functions are plotted (solid and dashed line respectively), the magnet lattice is represented schematically in the middle part and the horizontal and vertical dispersion in the lower part of the plot. The graphics demonstrate that matching onto the arc structure is possible for the described β^*-functions at the IP.

The minimum value of the horizontal beta function after the interaction region is adjusted to occur inside the middle of the first vertical acting main quadrupole located at a position of

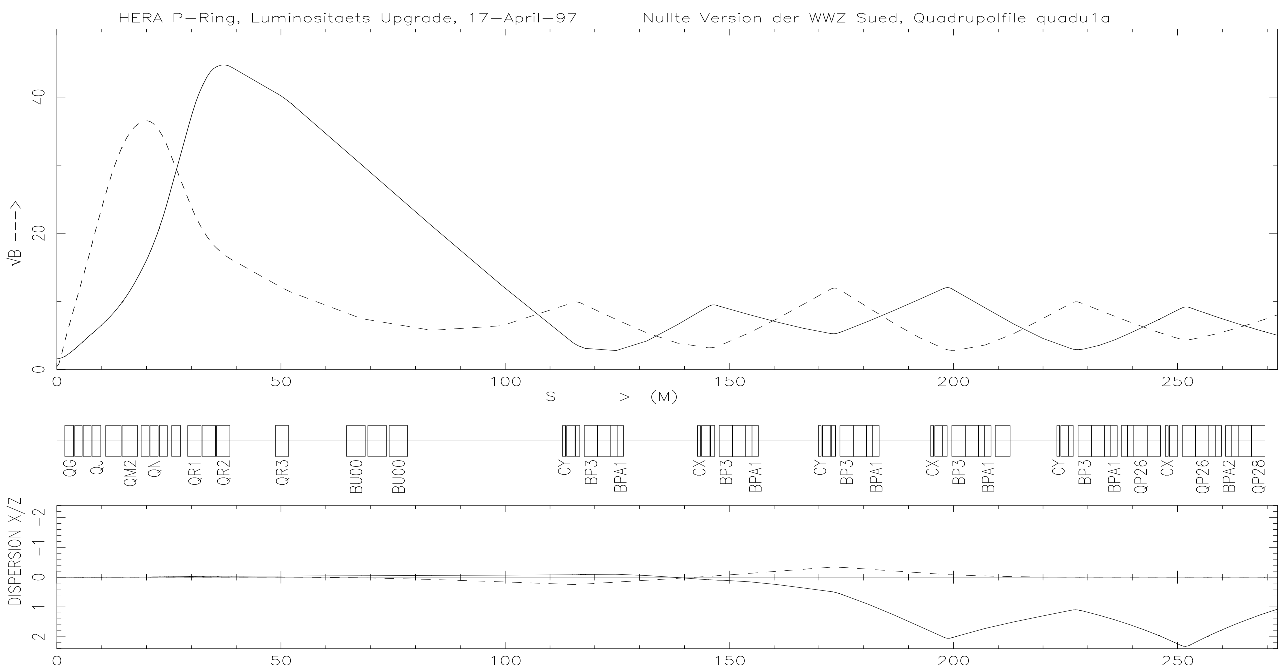

Figure 36: *First part of the new HERA-proton beam optics. For the values of the horizontal and vertical betafunction at the Interaction Point (beam coordinate s=0 in the plot) 2.45m and 0.18m were chosen in agreement with table 16.*

115 m. Large extensions of the twiss-parameters during the further matching onto the periodic optical solution in the arcs can be avoided this way. Clearly the same holds for the vertical plane as can be seen in Fig. 37 where the optical solution is presented embedded in the complete quadrant of the HERA proton ring.

Dispersion suppression is obtained by using the existing 'missing bend scheme' of the HERA proton ring. Seen from the arc where the horizontal dispersion is fluctuating periodically between 0.9m and 1.8m the dispersion is matched to zero at the interaction points North and South and only a little extension is needed at a distance of about 250 m from the IP where the horizontal dispersion reaches a value of about $D_x = 2.3\,m$

The vertical dispersion D_y which is created by the vertical bending of the proton beam is corrected locally. The phase advance between the vertically bending BU magnets and its counterpart BV which is used to bend the beam back into the horizontal plane is chosen to be exactly 180 degrees by proper matching the strength of the super-ferric correction quadrupoles 'QQ' located in that region.

Due to the stronger focusing needed for the reduced spot size at the IP the phase advance is increased inside the interaction region – compared to the present HERA-p design. Mainly in the horizontal plane this effect cannot be corrected by the use of the interaction region quadrupoles only. The optimum working point of the machine therefore is obtained by re-iterating the strength of the integrated superconducting correction coils, i.e. the 'QP' magnets. The tune is put close to the coupling resonance as in the present HERA design, namely to $Q_x = 31.292$ and $Q_y = 32.296$ in the horizontal and vertical plane, respectively.

The resulting periodic solution of the proton beam optics is only slightly differing from the present values. It is listed in the case of the 820 GeV luminosity case in table 17.

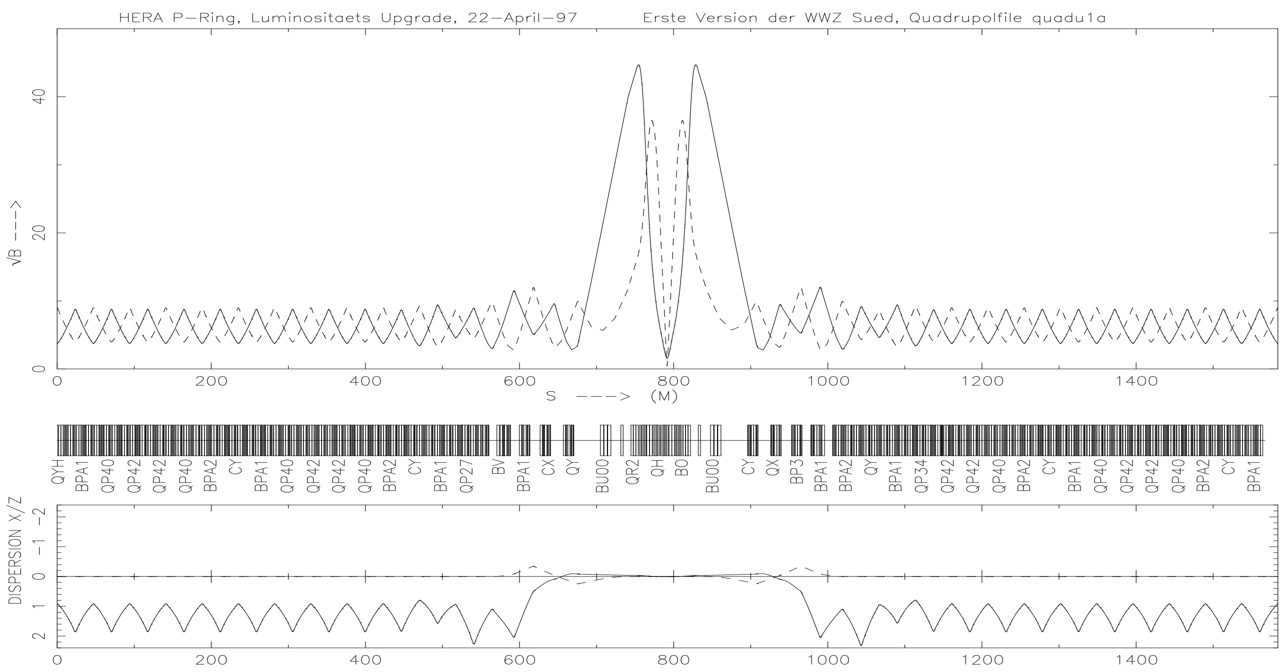

Figure 37: *Upgraded luminosity optics for the HERA-proton ring: The insertion starting at the Interaction Point at the center of the plot is embedded inside the periodical structure of the two neighboring octants left and right.*

	horizontal	vertical
beta function	12.1624 m	81.9948 m
alpha	-0.001	0.001
dispersion	0.80 m	-0.0006
derivative of dispersion	0.0	0.0

Table 17: *Optical parameters for the periodic structure in the HERA-p arcs obtained in the middle of a vertical focusing main magnet.*

For completeness the new designed interaction regions in the straight sections NORTH and SOUTH were inserted in the lattice of the complete ring and the whole optics re-matched slightly for exact boundary conditions at all 4 interaction points. The result is plotted in Fig. 38 which shows the full 820 GeV optics in the conventional sequence region EAST , SOUTH, WEST and NORTH.

6.5.3 Magnet Strengths

As the new designed luminosity optics is supposed to run at an energy of 820 GeV all the magnet strengths needed for the above mentioned beam optical solution have to be valid up to that energy. The needed quadrupole strengths are listed therefore in the table 18 below together with the corresponding magnet currents for the scheduled energy of 820 GeV and the given limitation of the maximum current allowed by the capability of the magnet or the cable feed-throughs.

In the case of the new designed magnet types the value of the required transport current depends on the detailed layout of the magnets which is explained elsewhere in this report. The

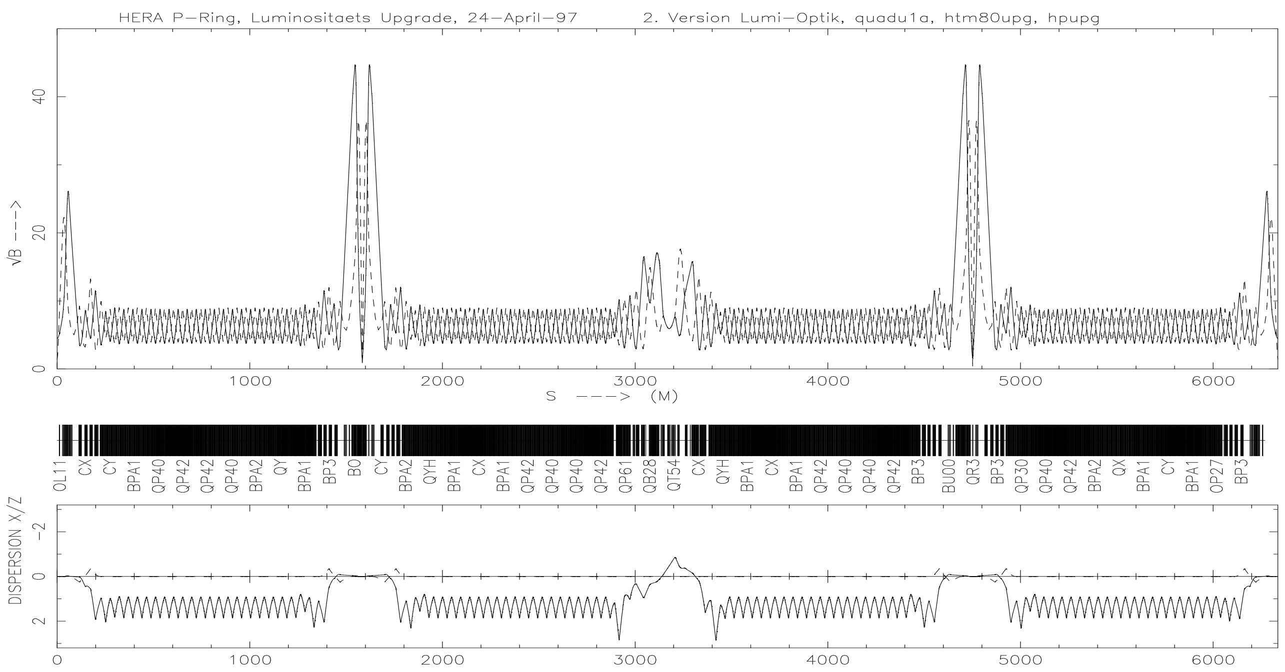

Figure 38: *Complete optical solution of the HERA proton ring for an upgraded Interaction region in the two sections NORTH and SOUTH. An optimized setting of the arc correction quadrupoles was found to compensate for the phase advance in the new IR's and the Interaction Regions EAST and WEST had to be re-matched slightly.*

required magnet strengths however as indicated in table 18 do not over pass the capability of these new quadrupole types.

magnet type	magnet strength $k(m^{-2})$	required current at 820 GeV	current limitation
QM1	$8.6 * 10^{-3}$	—	—
QM2	$8.6 * 10^{-3}$	—	—
QN	$1.0 * 10^{-2}$	—	—
QR1	$-8.5 * 10^{-3}$	472 A	490.0 A
QR2	$-4.7 * 10^{-3}$	262 A	490.0 A
QR3	$-1.5 * 10^{-3}$	85 A	490.0 A
QQ16 ... QQ25	$1.3 * 10^{-3} \ldots 5.6 * 10^{-3}$	6.3 A ... 27.4 A	100.0 A
QP26 ... QP34	$1.6 * 10^{-5} \ldots 4.5 * 10^{-4}$	2.1 A ... 59.7 A	100.0 A

Table 18: *Required strengths of the quadrupole magnets in the new designed interaction region. The current values are calculated for the 820 GeV flat top energy and compared to the existing limitations.*

6.5.4 Injection Optics

The proton beam is injected into the HERA proton accelerator at an energy of $E_0 = 40\,GeV$. Correspondingly the (non–normalized) emittance of the proton beam at injection is 20 times larger than at flat top energy. On the other hand the values of the beta-functions at the IP can be increased which reduces the peak values $\hat{\beta}$ drastically. This leads to completely different boundary conditions for the beam optics. Beside the fact that the 40-GeV optics has to match the optical parameters at the injection point and to guarantee the required phase relations at the proton dump system both located at section West, it is mainly the increased emittance at low energies that defines the boundary conditions at the interaction regions North and South:

Based on the assumption that the normalized emittance for 2σ is about $\epsilon = 20\pi\, mm\, mrad$ the absolute value of ϵ is at injection $\epsilon \approx 1.2 * 10^{-7}$ compared to $\epsilon \approx 6.0 * 10^{-9}\pi\, mm\, mrad$ in the flat top. So at both the superconducting and the normal conducting part the size of the beta functions has to be limited to guarantee enough free space at the low energy side of the machine.

In Fig. 39 a possible solution for an proton injection optics is shown for the first sequence of elements. It is based on the magnet lattice as presented in the previous section. As — unlike in the luminosity case — the value of the beta function at the IP can be chosen freely within the limits of the free aperture, it was used to define starting conditions that fit easily into the given interaction region geometry.

Requiring still symmetry conditions for the optics of one quadrant, i.e. the alfa values are set to zero, the best solution for the interaction regions are found for a beta function of

$$\beta_x = 15.30\, m \qquad\qquad \beta_y = 2.93\, m$$

in the horizontal and vertical plane, respectively.

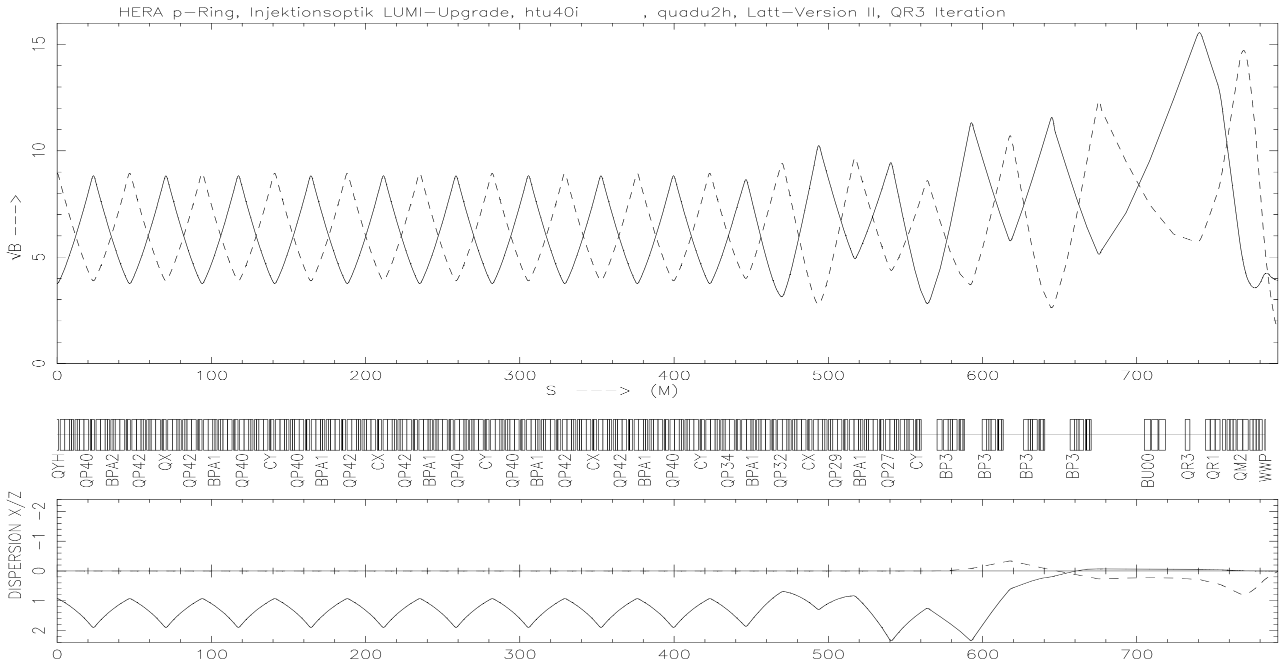

Figure 39: *p-beam optics in the left part of the interaction region, optimized for the injection energy of 40 GeV. At the interaction point which is located at a position of s=800 m in the plot of this figure the horizontal dispersion and the deviation of the beta function are matched to zero.*

As high peak values of the beta function namely in the horizontal plane have to be avoided, the optics has been optimized for a very first focusing of the horizontal beta function. For this purpose two lenses of the electron mini beta triplet magnets, 'QI' and 'QJ' are used to bend back the increasing horizontal beta function and to create a second minimum in β_x which avoids intolerable deterioration in the horizontal plane by the vertical proton mini beta magnets 'QM' and 'QN.'

The horizontal focusing is completed by the sequence of 'QR' magnets as indicated in Fig. 39, the maximum focusing strength — unlike to the luminosity optics — being shifted into the direction of the last normal conducting quadrupole magnet 'QR' to reduce the peak values of both amplitude functions in the following superconducting section.

In table 19 the resulting quadrupole strengths 'k' are indicated together with the required currents at the injection energy of $E_{inj} = 40\,GeV$ and an assumed energy of $E_{zwi} = 300\,GeV$ which is scheduled for the first acceleration step in the machine.

		required current		
magnet	strength $k(m^{-2})$	at 40 GeV	... at 300 GeV	max. current
QG	0.0	—	—	—
QH	0.0	—	—	—
QI	$-2.2 * 10^{-2}$	—	—	—
QJ	$-2.2 * 10^{-2}$	—	—	—
QM1	$5.2 * 10^{-3}$	—	—	—
QM2	$5.2 * 10^{-3}$	—	—	—
QN	$1.3 * 10^{-2}$	—	—	—
QR1	$-1.2 * 10^{-4}$	0.3 A	2.4	490.0 A
QR2	$-8.8 * 10^{-3}$	23.9 A	179.1	490.0 A
QR3	$-8.9 * 10^{-3}$	24.0 A	179.7	490.0 A
QQ16 ... QQ25	$2.0 * 10^{-3} \ldots 2.3 * 10^{-2}$	0.4 A ... 6.2 A	3.2 ... 46.4 A	48.0
QP26 ... QP34	$1.0 * 10^{-5} \ldots 5.3 * 10^{-4}$	0.1 A ... 3.4 A	0.5 ... 25.9 A	100.0 A

Table 19: *Quadrupole strengths required for the new injection optics based on the update–lattice presented above. The indicated magnet currents are calculated for the injection energy of 40 GeV and up to an intermediate energy of 300 GeV*

The free aperture inside the interaction region depends on both the available free bore radius of the newly designed magnets and the amplitude function of the beam optics which is valid in a given energy range. As the most critical part is the 40 GeV case the present status of the available aperture radii is listed in table 20 at injection energy where the highest emittance is found.
The values are obtained for a two sigma normalized emittance of $\sigma_n = 20\pi\, mm\, mrad$.

In Fig. 40 the new version of the injection optics has been inserted into the complete HERA-p optics.

magnet	$\beta_x(m)$	$\beta_y(m)$	$\sigma_x(mm)$	$\sigma_y(mm)$	$r_0(mm)$	number of σ_x	number of σ_y
QG	16.2	7.8	1.4	1.0	—	—	—
QH	17.4	13.9	1.5	1.3	—	—	—
QI	18.0	24.6	1.5	1.8	35	23.3	19.4
QJ	16.3	45.3	1.4	2.4	50	35.7	20.8
QM1	12.6	117.3	1.3	3.8	37	28.5	9.7
QM2	14.1	178.7	1.3	4.7	37	28.5	7.8
QN	34.2	215.7	2.1	5.2	35	16.6	6.7
QR1	139.9	144.0	4.2	4.2	35	8.3	8.3
QR2	172.5	81.9	4.6	3.2	35	7.6	10.9
QR3	237.9	35.9	5.5	2.1	35	6.3	16.6
QQ/QP	127.0	147.9	4.0	4.3	27	6.2	6.8

Table 20: *Aperture requirements for the p-beam stored at an energy of 40 GeV. The indicated beta-functions correspond to the above mentioned injection optics. The resulting beam diameters are based on an two sigma emittance of 20 π mm mrad.*

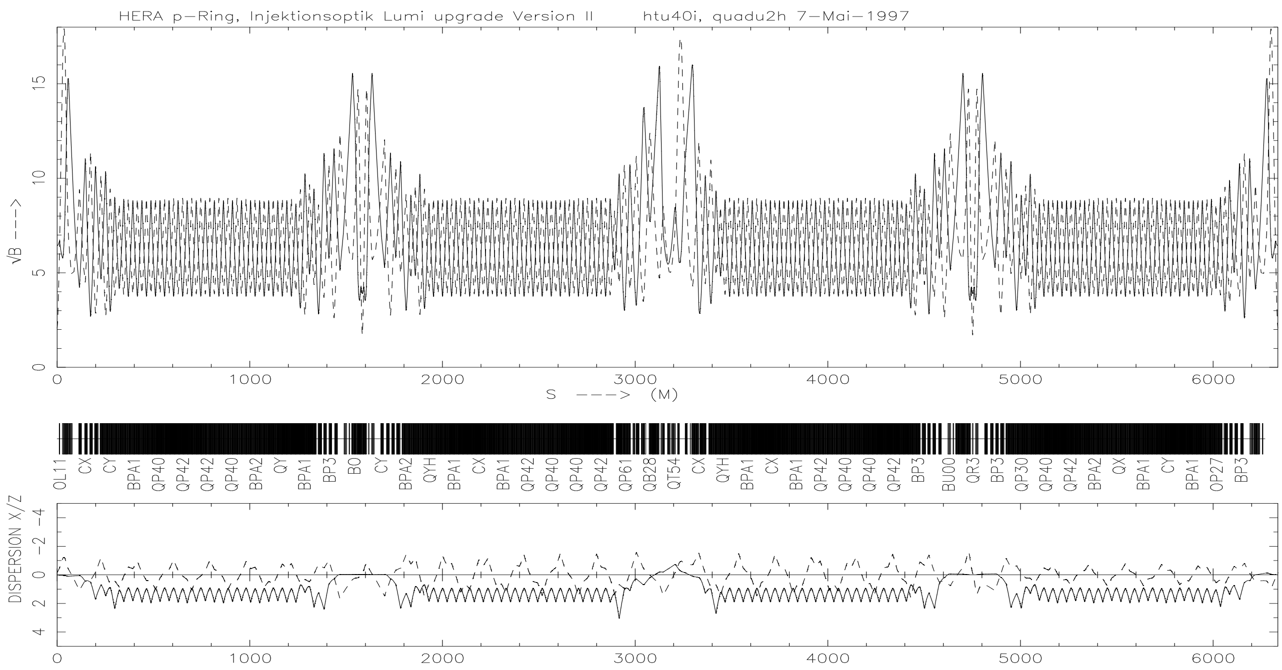

Figure 40: *P-beam optics at injection energy. The periodic solution of the beam optics optimized for the new interaction scheme is plotted for the compete HERA-p ring. The optics is shown in the usual manner starting at the symmetry point in hall EAST and following the structure through the interaction regions SOUTH, WEST and NORTH.*

6.5.5 Change of Proton Orbit during the Acceleration of the Positrons

During acceleration of the the leptons from injection energy of $12GeV$ to top energy (30GeV) the separator magnets and the low-β quadrupoles of the electron beam change their strengths from 60% to 100%. These field changes affect also the proton beam. In the present lattice, this is compensated by a $1.5m$ long septum magnet BS which is located in front of the proton low-β quadrupoles. This solution is not desirable in the upgraded lattice since the septum coil is thicker than the new quadrupole septum. Therefore, the lattice has been arranged such, that the changing fields which are experienced by the proton beam cancel each other as much as possible and the septum dipole will be obsolete.

In the following we are investigating the case of the **Rev2**-lattice with superconducting magnets. We limit ourselves to the e-downstream case since it is the worst case.

The superconducting magnets QG and QH are aligned along the detector axis. Since the proton orbit does not change noticeably, the protons see a constant field inside these magnets. The difference in deflection before and after lepton ramping is $kl \cdot x_p \cdot 18GeV/820GeV = 0.13mrad$. This is a kick directed outwards. The next two elements are the low-β quadrupoles QI and QJ which are aligned on the lepton orbit. The average separation between protons and positrons inside these magnets is $22.5mm$ and $37.5mm$ respectively. With k-values of $0.27m^{-2}$ and $0.20m^{-2}$ and lengths of $1.88m$ respectively, the protons experience another outward-kick from the weakened horizontally focusing QI of $0.23mrad$ and inward-kick of $0.29mrad$ from QJ. The proton orbit at the downstream end of QJ is shifted by $1.3mm$ outwards. This requires a proton optics with relaxed vertical $\beta^*_{yp} = 36cm$ during lepton acceleration in order to maintain an aperture of $12.5\sigma_{x,y}$. The difference kick is $0.075mrad$ at this point. This leads to a maximum orbit excursion of $6mm$ outwards in the last vertically focusing low-β quadrupole QN. The value of β^*_{xp} should be relaxed from $2.45m$ to about $3.6m$ during lepton acceleration as well to avoid effective aperture reductions. The orbit is bend back by the BO magnet before the horizontal low β quadrupoles QR and the offset is reduced in the horizontally focusing QR magnets were the aperture is limited in the horizontal plane. Fig 41 show an exact calculation of the the proton orbit change during acceleration of the leptons from $12GeV$ to $30GeV$.

6.5.6 Proton-Positron Collisions

In case of switching from electrons to positrons, the orbit of the protons inside of QJ changes by $5.2mm$. The orbit excursion inside the proton low-β magnets QN reaches up to $24mm$. This requires a different placement of the proton low-β magnets and switching between electrons and positrons will be much more difficult than in the present case. Also the aperture at the end of QI will be very tight, especially since in this case, the full luminosity optics will be needed. A solution to this problem would be a reduction of the separator kick to from $8mrad$ to $7mrad$ and and outward shift of QJ by $2.5mm$. This would provide half of the lost aperture and at the same time the excursion of the proton beam would be reduced by $\sim 1mm$. The synchrotron radiation fan would widen by about $5mm$ which is well inside the margin. This problems has not yet been explored in detail. It is obvious that switching between electrons and positrons will be more difficult in the upgraded lattice compared to the present one. Larger apertures of QJ will be desirable (which is being considered at present) to avoid a possible loss of luminosity or more difficult conditions with synchrotron radiation in the case of proton/positron operation.

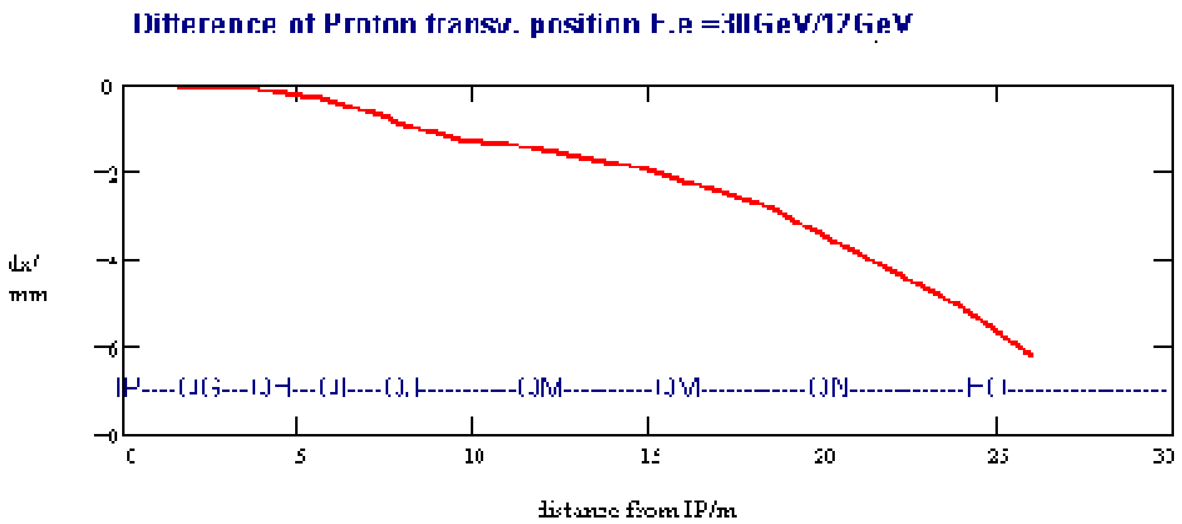

Figure 41: Proton Orbit Change during Ramping of the Leptons

6.5.7 Stability of the Proton Beam

In contrast to the stability issue of the lepton beam, there is less concern about the stability of the proton beam since the upgraded lattice does not require large changes in the sextupole strengths due to increased chromaticity. However, though the additional chromaticity is not very large, it is not negligible. Despite the fact that the peak-β values are even smaller than in the present HERA lattice, the chromaticity is still somewhat larger. The low-β quadrupoles are closer to the IP and therefore they must be stronger $kl \sim 1/s$ (s being the distance of the quadrupoles from the IP). The values are $\xi_x = -76$ and $\xi_y = -80$ which has to be compared to $\xi_x = -69$ and $\xi_y = -84$ for the present lattice with the 1997-optics. The corresponding change in dynamic aperture may be estimated in the following way:
First we consider a hypothetic case departing from the present situation. Suppose that the linear beam optics in the arcs would be unchanged (which is in good approximation indeed the case for the upgraded lattice), the β-tron phase advances across the straight sections would be the same (which is also true in good approximation for the new lattice). If the strengths $m \cdot l$ of the two sextupole families would be scaled by a common factor, then the dynamic aperture $\hat{x}$ for this configuration would scale obviously according to $\hat{x} \sim (m \cdot l)^{-1}$. Unfortunately, the change in chromaticity for the Rev2-lattice requires rescaling of the sextupole strengths with different scale factors for the two families. Thus the scaling law is not applicable. However if the strongest scale factor is taken as the common one, the resulting reduction of dynamic aperture might be considered as a conservative estimate. This gives a dynamic aperture reduction in the order of 10% for the Rev2 lattice compared to the present lattice. This reduction of dynamic aperture is considered to be tolerable.

Particle tracking calculations are being performed to confirm this estimate. Results are not yet available at this point.

6.6 Impact on e^+/e^- Polarization

6.6.1 Introduction

Polarization will remain an important issue for HERA. An increase of the luminosity should not spoil the polarization deliverable to HERMES and possibly to H1 and ZEUS. We describe here the impact of the new IP region design on the polarization with regard to so the called REV1 option. The REV2 solution has not yet been studied.

The shrinking of the space available with the new IP region design has two important consequences for polarization:

- the experimental solenoids will not, as at present, be compensated anymore by anti-solenoids;
- the experimental solenoids must overlap with the last machine magnets.

There exists no optics code able to handle this somehow exotic field configuration. We must therefore develop the appropriate tools to approach the problem.

In the actual HERA design the compensating anti solenoids have two important tasks: compensate for the betatron coupling and for the distortion of the closed solution of the BMT equation, $\hat{n}_0$, generated by the solenoids themselves. Their removal therefore has important consequences.

Clearly the H1 solenoid presents more difficulties for the machine than the ZEUS one, because it has a higher integrated field, is longer and longitudinally off center w.r.t. the IP. In the following we will therefore concentrate our attention mainly on the H1 solenoid; the solenoid parameters are taken from [1].

6.6.2 Effect of antisolenoid suppression on coupling.

Concerning the betatron coupling, the idea is to insert around each IP two pairs of symmetric and antisymmetric skew quadrupoles in order to compensate the real and the imaginary part (the solenoids are not centered w.r.t. the IP) of the driving term of the linear difference resonance. Of course, as the H1 and ZEUS solenoids are quite different, we will need different skew quadrupole settings in North and South.

6.6.3 Effect of antisolenoid suppression on $\hat{n}_0$.

Concerning the effect on the polarization axis direction $\hat{n}_0$, the REV1 solution, which foresees a longer drift at the experiment regions and weaker bending magnets around the IP, looks more convenient then the previous one [2].

Nevertheless corrections must be envisaged.

For this study we must distinguish whether at the solenoid location the nominal $\hat{n}_0$ direction is vertical or, by means of the spin rotators, longitudinal.

In the first case, once the solenoids are powered on, $\hat{n}_0$ will be tilted by several tens of milliradians (about 120 mrad through the H1 solenoid) around the longitudinal axis and the depolarization will be very strong.

Following[3], we looked at the feasibility of a compensation scheme consisting of two vertical bumps antisymmetric w.r.t. the IP and involving the two bending magnets BB01. The second vertical bending magnet should provide an orbit kick of 2.5 mrad resulting in a maximum orbit excursion of about 10 mm.

Such vertical bumps could be realized also by making use of the rotator magnets, if already installed; they should run at about 60% of their nominal value.

In the case that the rotators are operating, we have already seen[2] that we must compensate for the fact that $\hat{n}_0$ is not yet perfectly longitudinal when entering the experimental solenoids and that the solenoids are not centered w.r.t. the IP.

At 27.5 GeV, the residual tilt at the H1 solenoid exit will be about 13 mrad. This is about a factor 2 smaller than quoted in[2]; this improvement is mainly due to the smaller overlap between the machine bending field and the solenoid field of the detector.

We have proved that a slightly different setting of the rotator vertical bending magnets on the left and on the right side of the IP would be able to reduce the tilt due to the H1 solenoid to less than 1 mrad. Table 21 shows the orbit kicks needed for the compensation at 27.5 GeV as well as, for comparison, the nominal values.

6.6.4 Spin diffusion in presence of rotators.

Once we have for $\hat{n}_0$ a closed solution vertical in the arcs, we must still consider the effect of having a beam of finite dimensions circulating in a machine with a non zero vertical dispersion and with non vertical $\hat{n}_0$ in large sections of the ring.

Referring the reader to [4] for more details, we say here only that, in order to minimize the resulting spin diffusion, we must design a spin matched optics: to the usual optical constraints we must add conditions for getting a spin transparent machine. For this purpose we design the optics by using the code SPINOR [5].

The REV1 optics proposed for the luminosity upgrade of the HERA e^+/e^- ring, with 90/60 degrees phase advance in the FODO cells and with three pairs of spin rotators (East, North and South), has been spin matched at 27.5 GeV.

It is worth noting that in this solution the spin matching of the synchrotron motion along the straight sections North and South has been obtained by moving the BI01 magnet from the current position to 110 m from the IP. This would imply a radial shift of the interaction point. Whether such a shift is really unavoidable will be investigated later on.

	H1 solenoid ON	nominal
BF left	9.578 mrad	9.841 mrad
BG left	13.292 mrad	11.552 mrad
BF right	9.892 mrad	9.841 mrad
BG right	11.721 mrad	11.552 mrad

Table 21: Rotator vertical bend settings

In spin matching the optics we ignored the presence of the experimental solenoids. The idea is that the perturbation introduced by the solenoids, is still small enough not to modify substantially the $\hat{n}_0$ axis direction along the straight sections when the rotators are operating.

The solid line in Fig. 42 shows polarization versus energy for an ideal machine and in linear spin motion approximation; the three dashed lines correspond to the polarization related to the three degrees of freedom of the motion separately. We can see that the maximum polarization achievable is limited by the synchrotron motion.

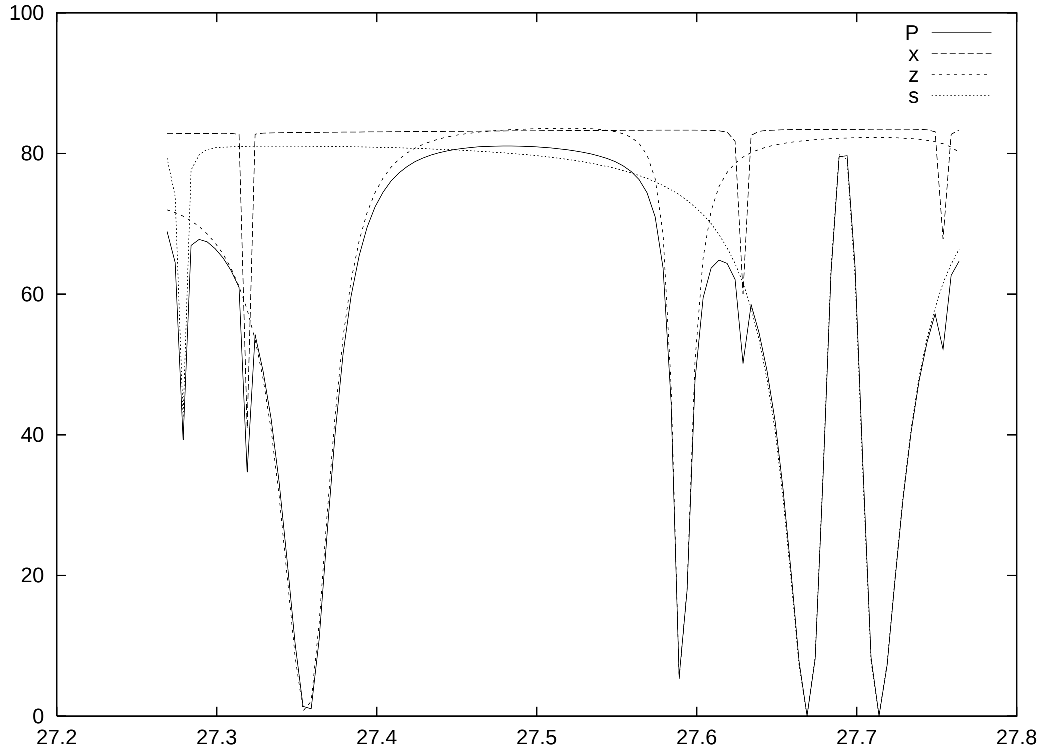

Figure 42: Polarization vs. Energy with 3 Rotators on.

These results are obtained ignoring the presence of the experimental solenoids, under the assumption that their effect on $\hat{n}_0$ direction and on coupling have been already well compensated, as explained in the previous subsections.

These assumptions must be verified once we can model the field configuration in our code. For this purpose two ideas are being pursued:

1. Represent the superposition of horizontal bending magnet and straight solenoid along the curved ideal trajectory as an interleaved sequence of pure vertical and horizontal bending magnets and solenoids.

2. Use previously computed spin–orbit transfer matrices to represent the region of complicated overlapping fields.

Work on this topic is in progress.

References

[1] D. P. Barber, J. Roßbach, DESY HERA Report 86-13 (1986).

[2] G. Ingelman, A. De Roeck, R. Klanner (ed.), "Future Physics at HERA", Proc. Workshop 1995/96, vol.2, pag. 1124.

[3] K. Steffen, DESY M-82-25 (August 1982).

[4] J. Buon and K. Steffen, DESY HERA Report 85-09 (1985).

[5] D. P. Barber, L. Hand, unpublished.

7 Synchrotron Radiation and Experimental Background Analysis (D. Pitzl)

7.1 Synchrotron Radiation Analysis

7.2 Background from lost Particles

7.3 Specification of Absorbers and Masks

7.4 Synchrotron Radiation at the ZEUS Interaction Region (Rev1 Lattice)

The electron beam traversing the magnets in the interaction region is a strong source of synchrotron radiation. The direct radiation beam, which spans an angle of ± 8 mrad has to stay clear by 5 mm of any surface in the vicinity of the experiment. Its power, at an electron energy of 30 GeV and 58 mA beam current, is 25 kW (both sides). The critical energy is 100 -150 keV. In addition, one has to consider radiation from the quadrupoles QI and QJ which are upstream of the first separator magnets. This radiation has a power of about 70 W and a lower critical energy of about 70 keV. Nevertheless it should also not touch anything inside the interaction region. For example, trying to stop the radiation by a 1 cm thick collimator at z=0.8 m, will produce 0.1 W of edge scattering for an assumed incident horizontal power density of 4 W/mm ($6 \cdot 10^{14}$ photons/mm). This value is too large by a factor 100-1000. The radiation has dropped to an acceptable value at a distance of 29 (55) mm from the beam center at 1.6 (0.8) m upstream (downstream) of the interaction point, and it has a vertical (total) width of 1.5 mm at the latter position. The horizontal and vertical beam profiles, including the quadrupole radiation, at a distance of 0.8 m downstream from the interaction point, are shown in Fig 43. Avoiding to touch anything of these direct beams, the main background in the experiment then comes from the radiation backscattered from the main absorbers, situated between 11 and 27 m downstream from the interaction point.

Actually, the following sources of background from synchrotron radiation have to be considered:

1. Backscattered radiation from the main absorbers at 11 to 27 m from the IP.

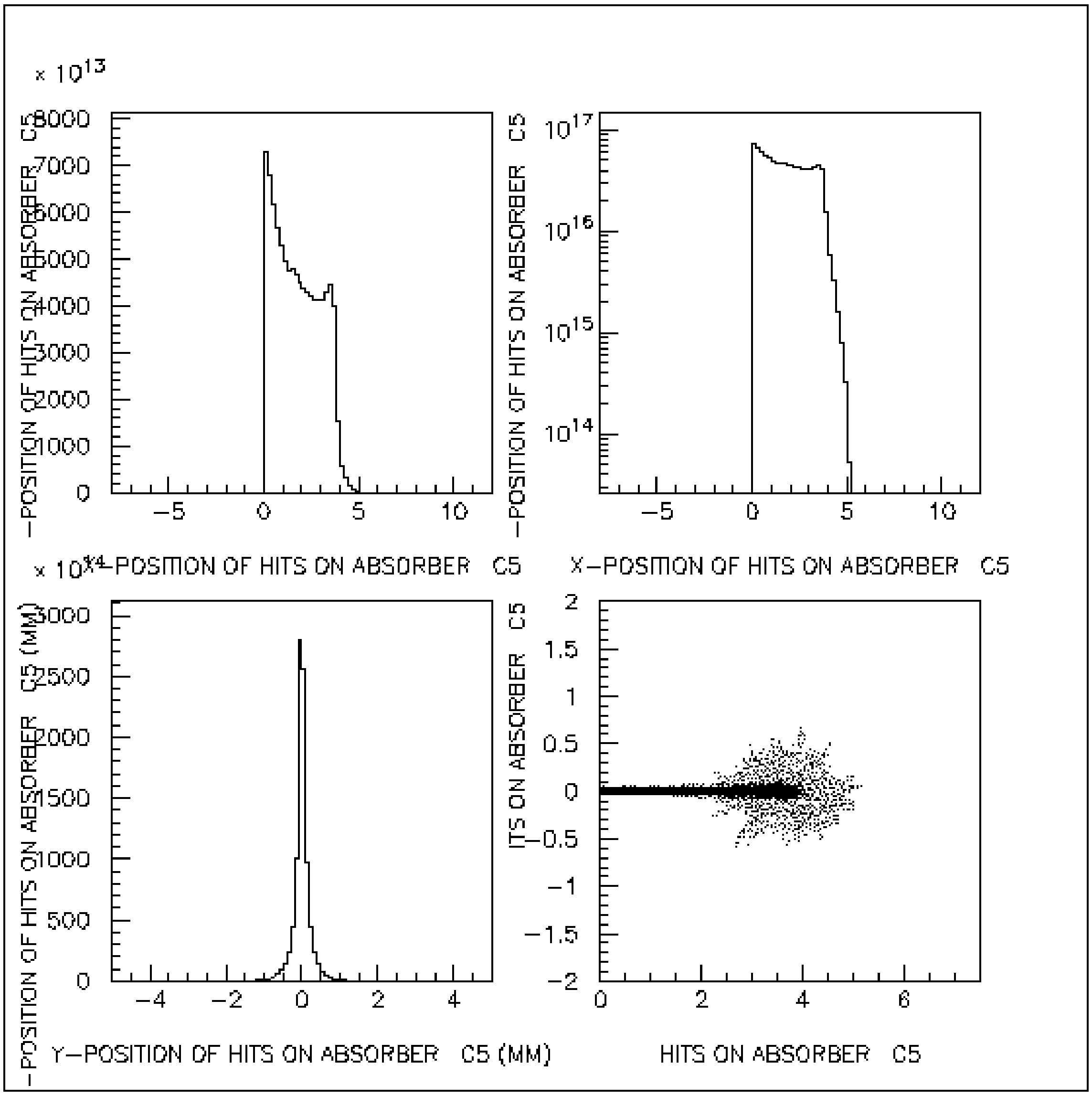

Figure 43: Synchrotron radiation fan at collimator C5 located at 0.8 m.

2. Edge scattering from absorbers near the IP, designed to protect the experiment against source 1).

3. Radiation reflected from the main absorbers, which is then diffusely reflected from the beam pipe walls into the detector.

Only the first source, which should give the main contribution, will be treated.
Fig. 44 shows the interaction region with the normal conducting magnets of Rev1 with a line marking the direct radiation. It is not touched by any absorbers until it hits the main absorbers. A safety distance of 5 mm should be kept for all surfaces. The back reflected radiation constitutes the main background. All sensitive parts of the detector have to be shielded from it. This is done by absorbers placed at z = -1.36 m and z = -0.8 m from the IP. These absorbers have to leave space for the radiation from the quadrupoles, which is outside the 8 mrad line. A keyhole-like opening may achieve this. In addition another absorber 1.5 m

upstream of the interaction point may be required, which has to stay outside of the quadrupole radiation, and provides shielding from more stray radiation from upstream magnets.

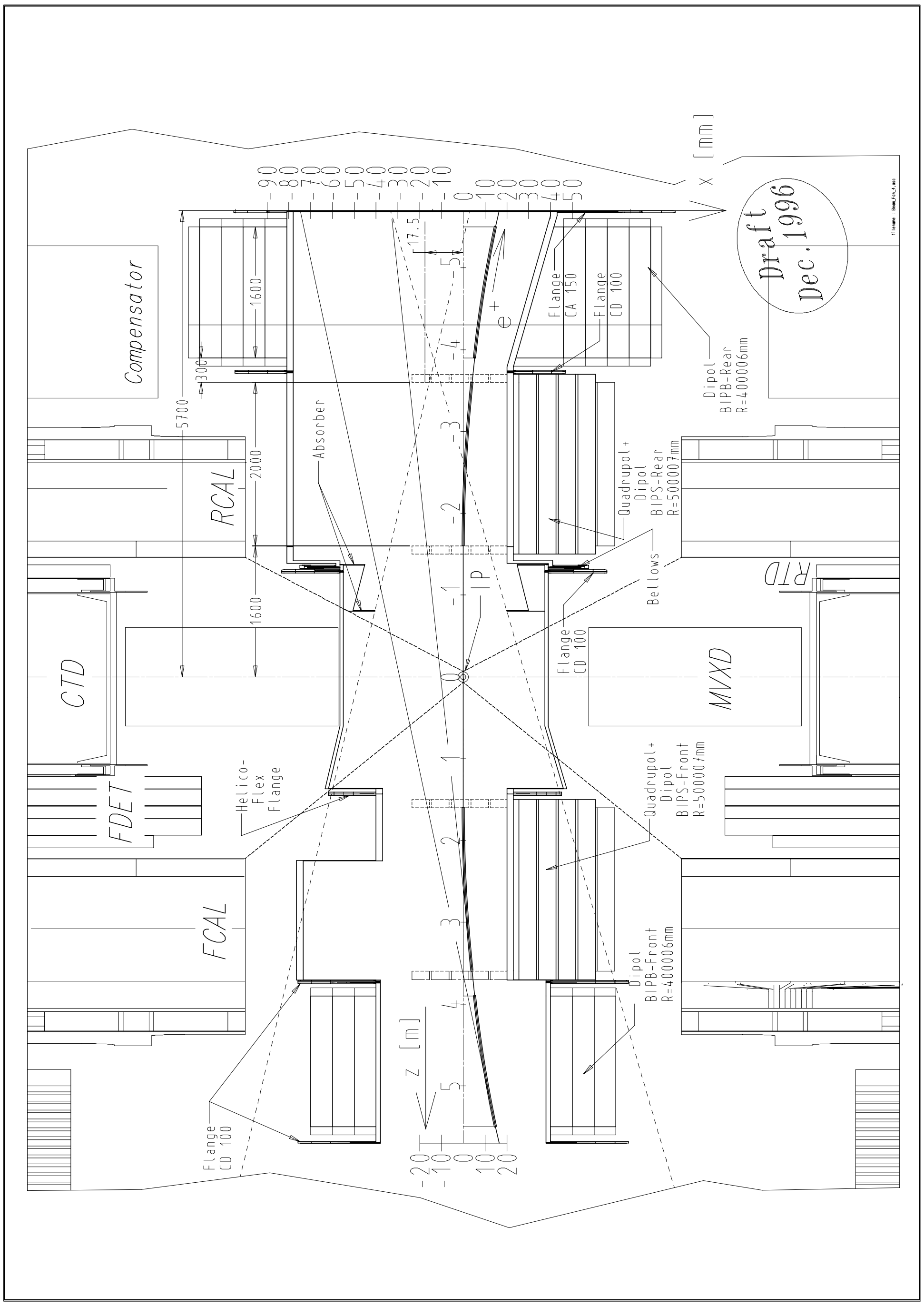

Figure 44: Sketch of the IP layout with normal conducting magnet (Rev1). The direct 'dipole' synchrotron radiation is displayed (no quadrupole tails).

In order to estimate the synchrotron radiation background, scaling from the present running conditions is the most accurate procedure. For this comparison we assumed the same electron energy, namely 30 GeV and the same current of 58 mA.

Table 22 gives a summary of this comparison for the power incident on the absorbers.

	present	upgrade	factor
Total Power	9.7 kW	24.6 kW	
Power on absorbers	5.1 kW	21.2 kW	
normalized to 23 m	5.1 kW	29.0 kW	5.7
symmetric quad coil	5.1 kW	32.9 kW	6.5

Table 22: Comparison of total synchrotron radiation power

Table 22 lists in the first row the total synchrotron radiation power, and on the second row the power hitting the absorbers. (The rest of the power continues and its influence on the interaction region is neglected). To get a comparison of the present/upgrade situation, the radiation from the absorbers has been normalized to a distance of 23 m, assuming a $1/r^2$ law.

Two absorber arrangements were considered:

1. standard design with the quadrupole coils split in magnet QN (3rd row),
2. QN quadrupole with normal symmetrical coils (4th row).

There is a difference in the reflected power of 14%, which is probably not large enough to justify the more complicated quad design of version 1). Summarizing, the power level is increased by a factor 6.5 for the upgrade version.

Next one has to consider the change in the reflection coefficient due to the difference in critical energy, and due to the different angle of incidence. Presently the angle of incidence is $\approx 90°$,whereas for the upgrade one needs grazing incidence at an angle of 40-100 mrad. The following table lists reflection coefficients, for the two reference cases, at critical energies of 40 and 140 keV (average), respectively.

reflection	critical energy	antirefl.coating	in 2π sr	back reflect./sr
90°	40 keV	no	1.4%	0.6%
90°	140 keV	no	3.3%	1.1%
40-100 mrad	140 keV	no	18%	$0.56 \pm 0.13\%$
40-100 mrad	140 keV	yes	10%	$0.27 \pm 0.06\%$

Table 23: Reflected synchrotron radiation

Table 23 shows, that at grazing incidence a large fraction (18%) of the incident radiation is reflected. It must be taken care of by a proper design of the absorber region. It is also seen, that an antireflection coating of 30μm Cu, 30μm Ag, and 500μm W on Cu will probably work and reduce the reflection by about a factor 2.
Overall, the percentage of reflected radiation seems similar for the present/upgrade schemes, because there is relatively less backward reflection for grazing incidence; this part of the comparison carries a factor 1.

The back reflected radiation is not allowed to hit any detector parts. Only after one more reflection, radiation is scattered into the detector. Here one gets a factor of 1.5 for the ratio of reflection coefficients, due to the difference of the mean reflected energy. These absorbers must be covered by an antireflection coating of 130μm Cu and 500μm Ag on W.

There are still two more differences: 1) In the present arrangement the collimators C1, C2 and C3 absorb about 50% of the power, decreasing the amount of power listed in table 23. On the other hand these absorbers are scattering additional background into the experiment. Assuming that these two influences approximately cancel, one gets a factor of 1 with an upper bound of 2.

The overall ratio of radiation backgrounds is therefore $6.3 \cdot 1 \cdot 1.5 \cdot 1 = 10$; i.e. we have to expect a level of radiation about 10 times larger than at present, normalized to the same electron beam current.

What are the consequences for the ZEUS detector?
The direct reflected synchrotron radiation delivers a dose rate of about 0.01 Gy/s, adding up to about 10^4 to 10^5 Gy/y. The vertex detector, which must of course be shielded from this radiation, receives a dose which is about 1000 times smaller.

The background in the CTD under present running conditions is small and hard to measure. One finds for the average number of background hits per event, which are more or less uniformly distributed through out the drift chamber:

$$N_{hit} = 1.75 + (0.037 \pm 0.016)\frac{I}{\mathrm{mA}}$$

With an electron current of I=58 mA, and a factor of 10, one expects 25±10 hits, which appears tolerable.

8 Magnet Design

8.1 The Rev1 Magnet Configuration

A schematic representation of the Rev.1 magnet configuration to the left of the IP is shown on Fig. 45 and for the right on Fig. 46 for the ZEUS and H1 experiments. For the Rev.1 lattice the two experiments differ on the left by having an air–core combined function magnet, QH1, for H1 and an iron dominated combined function magnet, QH, for ZEUS. This difference is necessitated both by the more restricted space in H1 at this magnet location and the presence of a large longitudinal magnetic field, which would immediately saturate an iron–dominated magnet. On the right side of both experiments an existing solenoidal compensator magnet is removed and this yields sufficient space on the right for the iron dominated combined function magnet, QH. Thus the ZEUS magnet configuration is left–right symmetric with QH on both sides. The configuration for H1, while functionally symmetric, does differ in having QH1 on the left and QH on the right.

The electron and proton beams are separated into separate beam pipes at ±11 m in the magnetic septum quadrupole QM. The inner combined function magnets QG and QH provide some central focusing for the electrons as well as the 8 mrad separation angle between the beam lines. The QI and QJ quadrupoles complete the inner focusing for the electrons and are